







## Article

# The Valorisation of Biochar Produced from Black Liquor Pyrolysis for the Development of CO<sub>2</sub> Adsorbents

Anca Maria Zaharioiu <sup>1</sup>, Violeta-Carolina Niculescu <sup>1,\*</sup>, Claudia Sandru <sup>1</sup>, Stefan Ionut Spiridon <sup>1</sup>,  
Amalia Soare <sup>1</sup>, Simona Oancea <sup>2</sup> and Florian Marin <sup>1,2,\*</sup>

<sup>1</sup> National Research and Development Institute for Cryogenic and Isotopic Technologies—ICSI Ramnicu Valcea, 4th Uzinei Street, 240050 Ramnicu Valcea, Romania; anca.zaharioiu@icsi.ro (A.M.Z.)

<sup>2</sup> Faculty of Agricultural Sciences, Food Industry and Environmental Protection, “Lucian Blaga” University of Sibiu, 7-9 I. Ratiu Str., 550012 Sibiu, Romania

\* Correspondence: violeta.niculescu@icsi.ro (V.-C.N.); florian.marin@icsi.ro (F.M.)

**Abstract:** The paper manufacturing process produces liquid and gaseous alternative fuels, as well as solid wastes. These can be subsequently treated through chemical processing, oxidation, and thermal activation, resulting in adsorbent materials with CO<sub>2</sub> adsorption capacities. The valorisation of black liquor waste resulting from paper manufacturing was achieved through a catalytic pyrolysis process using two catalysts previously prepared in house (Cu-Zn-MCM-41 and Ni-SBA-16). The HCl-treated adsorbent material, resulting from Ni-SBA-16-catalysed pyrolysis, was selected for use in CO<sub>2</sub> adsorption tests as it had the highest specific surface area (224.06 m<sup>2</sup>/g) and pore volume (0.28 cm<sup>3</sup>/g). The adsorption experimental setup was linked to a gas chromatograph in order to evaluate CO<sub>2</sub> adsorption efficiency using a binary gas mixture consisting of 81% CO<sub>2</sub> and 19% N<sub>2</sub>. With a CO<sub>2</sub> adsorption capacity of 1.61 mmol/g, a separation efficiency of 99.78%, and a CO<sub>2</sub> recovery yield of 90.02%, it can be concluded that the developed adsorbent material resulting from Ni-SBA16-catalysed pyrolysis and HCl treatment represents a viable solution for black liquor pyrolytic solid waste removal and reduction in greenhouse gases.

**Keywords:** adsorbent; black liquor; biochar; catalysis; pyrolysis



**Citation:** Zaharioiu, A.M.; Niculescu, V.-C.; Sandru, C.; Spiridon, S.I.; Soare, A.; Oancea, S.; Marin, F. The Valorisation of Biochar Produced from Black Liquor Pyrolysis for the Development of CO<sub>2</sub> Adsorbents.

*Molecules* **2024**, *29*, 5613.

<https://doi.org/10.3390/molecules29235613>

Academic Editor: Xin Liu

Received: 14 October 2024

Revised: 25 November 2024

Accepted: 25 November 2024

Published: 27 November 2024



**Copyright:** © 2024 by the authors. Licensee MDPI, Basel, Switzerland. This article is an open access article distributed under the terms and conditions of the Creative Commons Attribution (CC BY) license (<https://creativecommons.org/licenses/by/4.0/>).

## 1. Introduction

One of the main causes of climate change is the increase in the concentration of greenhouse gases, which is due to the irrational consumption of fossil fuels in rising quantities. The main greenhouse gas is CO<sub>2</sub>. The emission of this gas causes major concerns and is responsible for the increase in global warming by more than 50% [1]. The concentration of CO<sub>2</sub> in the atmosphere has increased rapidly, growing by over 100% compared to the base considered year—1850 [2]. Greenhouse gases are produced by various sectors, including industry, transport, and agricultural sector. This has led to the current CO<sub>2</sub> concentration of approximately 400 ppm [3,4].

Global warming, the deterioration of the Earth’s climate, and the destruction of habitats have had a series of consequences, such as an increase in the temperature at the terrestrial level and an increase in the temperature at the level of the seas and oceans. These effects have caused the melting of glaciers, floods, fires, and extreme meteorological phenomena [5,6]. The global temperature may increase by 1.5 °C until 2030, and by 2 °C until 2050, as was predicted by the Intergovernmental Panel on Climate Change (IPCC). In 2015, the Paris Agreement, an international agreement signed by 196 countries making a legal commitment to reduce greenhouse gases, was sealed [7]. The Paris Agreement requires a significant reduction in CO<sub>2</sub> concentrations in the atmosphere to prevent the global temperature from increasing. It proposes various measures and initiatives for the development of alternative, sustainable, and renewable fuels with increased energy efficiency to enable the replacement of fossil fuels, but also the capture of CO<sub>2</sub> [8,9].

CO<sub>2</sub> capture presents practical and economic advantages. CO<sub>2</sub> capture can be achieved through various techniques, and it is possible to capture it before and after the combustion process. The process of CO<sub>2</sub> capture and its conversion into value-added products has been promoted in recent years and is achieved through the development of functional materials such as adsorbents and catalysts [10–13].

Adsorbent materials developed from activated carbon were proved to be efficient for CO<sub>2</sub> capture. This is due to their properties such as high specific surface area, increased adsorption capacity, and low costs. Carbon materials can be used in various fields of technology due to their properties such as resistance to wear and tear [14]. Over time, activated carbon was obtained from coal, wood and oil, but currently other raw materials are being investigated, such as industrial waste from sewage sludge, [15], bone meal [16] and black liquor, which is a waste from paper manufacturing. The preparation of adsorbent materials requires chemical, physical, and thermal activation to increase their adsorption capacity and the development of cavernous pores [17,18].

Black liquor (BL) is a waste resulting from the paper manufacturing processes. It is a complex viscous solution containing organic and inorganic materials. These are represented by lignin and residual alkaline salts [19,20]. In this study, black liquor waste was subjected to a pyrolysis process carried out at two temperatures, 300 °C and 450 °C, in an inert nitrogen atmosphere and in the absence of oxygen. This process was performed in the presence of bimetallic MCM-41 (Mobil Composition of Matter No. 41) and monometallic-SBA-16 catalysts (Santa Barbara Amorphous), resulting in three types of pyrolysis products: liquid products (bio-oil—BL<sub>PYOIL</sub>), gaseous products (syngas—BL<sub>PYGAS</sub>), and solid products (biochar—BL<sub>PYCHAR</sub>) [20].

The literature mentions that different catalysts have been explored in pyrolysis to enhance the quality of the resulting bio-oil [21]. Various studies have only focused on the incorporation of catalysts such as NiO, MoO<sub>2</sub>, and Co<sub>3</sub>O<sub>4</sub> in a nitrogen atmosphere to reduce biochar formation and improve the properties of bio-oil [22]. When hydrogen was present, these three catalysts could enhance lignin degradation and boost bio-oil yield. Notably, Co<sub>3</sub>O<sub>4</sub> significantly improved lignin catalytic pyrolysis in a H<sub>2</sub>/N<sub>2</sub> atmosphere, resulting in a 26.38% increase in bio-oil yield [22]. Also, the pyrolysis of lignin from black liquor was improved with the addition of large-pore mesoporous materials (SBA-15) as catalysts and unilamellar mesoporous MFI nanosheets. Py-GC/MS was employed for analysis. It was observed that the quality of bio-oil was enhanced, with an increase in the quantities of aromatics and lighter phenolics, due to processes such as dehydration, decarbonylation, decarboxylation, and cracking, which occurred on the catalyst's acid sites [23]. Taking all these factors into consideration, the present study focused on enhancing the quality of the resulting biochar in order to further valorise it as adsorbent material.

The introduction of the MCM-41-type mesoporous molecular sieve in 1992 represented a significant advancement in using these materials as supports for different catalytic species [24]. This material possessed high specific surface areas (around 1000 m<sup>2</sup>/g) and well-defined pore dimensions (2–30 nm), a relatively narrow pore size distribution, and a hexagonal arrangement of parallel mesopores. By controlling synthesis parameters (template selection, reaction temperature and time, or pH), high-quality MCM-41 can be achieved, improving characteristics like high specific surface area, pore volume, uniform pore size distribution, and thermal and chemical stability [21]. The addition of different metals, such as Al, Co, Cu, Fe, and Ni, has been demonstrated to enhance the catalytic properties of this nanomaterial [21,25]. MCM-41 can act as an effective support for dispersing Ni active sites due to its high specific surface area. However, it is unable to prevent the agglomeration of metallic nickel nanoparticles at elevated temperatures, as its pore diameters are smaller than those of the metal particles [26]. To overcome this issue, a cubic three-dimensional SBA-16-type silica can be effective at dispersing Ni nanoparticles [26]. SBA-16-type silica possesses robust pore walls, a high surface area, and excellent thermal and hydrothermal stability [27]. Additionally, as an all-silica material, MCM-41 has Si–OH groups on its surface that offer only a limited number of weak acid sites, restricting deoxi-

dation and cracking capabilities during the pyrolysis process [28]. Consequently, several researchers have explored metal modification approaches, which can enhance both the structure and acidity of zeolite catalysts and improve catalytic performance and stability. Furthermore, this approach is becoming a promising method for upgrading bio-oil in biomass thermochemical processing. Also, when working with MCM-41, different metal was chosen to obtain the catalyst due to the fact that the Ni-MCM-41 did not have efficient catalytic effect on pyrolysis [28]. Furthermore, Cu-modified catalysts such as Cu/MCM-41 were reported to be efficient for upgrading bio-oil [29]. It was found that Cu incorporation effectively adjusted the acidity and textural properties of MCM-41, enhancing its deoxygenation capacity [29]. In this respect, a more efficient system (bimetallic Cu-Zn/MCM-41) was developed in this study, in which Zn was used as a promoter, in order to improve and overcome the above-mentioned limitations of MCM-41 catalysts.

The aim of this investigation was the removal of biochar resulting from the BL pyrolysis process. The necessity of removing biochar results from its high metal content and negative impact on the environment. BL<sub>PYCHAR</sub> elimination, performed by valorisation, involves its transformation into an adsorbent material through chemical and thermal processes [30–32]. The final objective was CO<sub>2</sub> removal and the identification of the adsorption capacity of the adsorbent materials prepared from the solid waste.

## 2. Materials and Methods

### 2.1. Adsorbents Preparation

The BL was procured from a pulp and paper factory (Drobeta-Turnu Severin, Romania), a kind of manufacturing that processes hard woods.

The pyrolysis process was carried out in a fixed-bed reactor. The temperature was controlled from 300 °C to 450 °C, with a temperature gradient of 5 °C/min, in an inert atmosphere (N<sub>2</sub>/5.0). The flow rate of the inert gas, N<sub>2</sub>, was 100 mL/min. Three products resulted from the pyrolysis process: a gaseous product—BL<sub>PYGAS</sub>; a liquid product—BL<sub>PYOIL</sub>; and a solid product—BL<sub>PYCHAR</sub>. These can be considered alternative fuels. The first two products were the subject of the initial study [25].

The BL<sub>PYCHAR</sub> was ground to a particle size <200 μm. After grinding, the chemical activation stage began. This was initiated by BL<sub>PYCHAR</sub> treatment with 5 M HCl and KOH (Sigma Aldrich, Darmstadt, Germany) in a 1:1 ratio.

The catalysts used in the BL pyrolysis were two catalysts that were previously prepared in house (Cu-Zn-MCM-41 and Ni-SBA-16) [25]. These produced two types of biochar, denoted as 1a—BL<sub>PYCHAR\_Cu-Zn-MCM-41</sub> and 1b—BL<sub>PYCHAR\_Ni-SBA-16</sub>. These two biochar materials constituted the raw materials for the development of the adsorbents. For the adsorbent's development, HCl and KOH (Sigma Aldrich, Darmstadt, Germany) were used in the chemical activation process. Five adsorbents (Table 1) were developed from BL<sub>PYCHAR</sub>: two were produced after HCl treatment (2a—BL<sub>PYCHAR\_Cu-Zn-MCM-41\_HCl</sub> and 2b—BL<sub>PYCHAR\_Ni-SBA-16\_HCl</sub>); two were produced after HCl and KOH treatment (3a—BL<sub>PYCHAR\_Cu-Zn-MCM-41\_HCl+KOH (1:1)</sub> and 3b—BL<sub>PYCHAR\_Ni-SBA-16\_HCl+KOH (1:1)</sub>); the fifth adsorbent was obtained after HCl and KOH treatment, followed by calcination (4a—BL<sub>PYCHAR\_Ni-SBA-16\_HCl+KOH<sub>c</sub></sub>). The calcination was carried out at a temperature of 750 °C, with a gradient of 10 °C/min, for 1 h in a N<sub>2</sub> atmosphere at a flow rate of 100 mL/min.

**Table 1.** The nomenclature of the adsorbents obtained as a function of treatment.

Treatment	Adsorbent Material
HCl	2a—BL <sub>PYCHAR_Cu-Zn-MCM-41_HCl</sub> 2b—BL <sub>PYCHAR_Ni-SBA-16_HCl</sub>
HCl and KOH	3a—BL <sub>PYCHAR_Cu-Zn-MCM-41_HCl+KOH (1:1)</sub> 3b—BL <sub>PYCHAR_Ni-SBA-16_HCl+KOH (1:1)</sub>
HCl, KOH, calcination	4a—BL <sub>PYCHAR_Ni-SBA-16_HCl+KOH<sub>c</sub></sub>

After the thermal activation process, the materials obtained were subjected to a filtering process using filter paper type 389 (84 g/m<sup>2</sup>; particle retention 8–12 µm; thickness 0.19 mm) (Sartorius Stedim, Gottingen, Germany). The materials were washed with distilled water until pH 6, and then dried in an oven (Nahita 631, Auxilab, Navarra, Spain) without ventilation. The drying was carried out in two steps to avoid shocks on the pores of the formed materials: it was performed at 70 °C for 12 h and at 105 °, for 6 h. After the drying process, the obtained material was pelletized using a pelletizer (IKA, Staufen im Breisgau, Germany). The pellets had a mass of approximately 1 g (Figure 1). Then, they were subjected to a drying process at a temperature of 105 °C for 4 h.

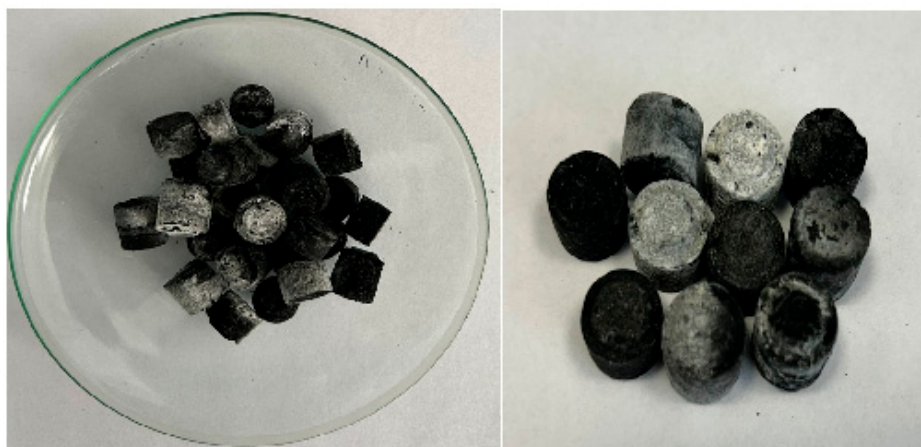


**Figure 1.** Black liquor char pellets.

## 2.2. Characterization of Biochar and Adsorbent Materials

The adsorbent materials were subjected to structural investigations such as elemental analysis, the determination of the heavy metal content, the determination of the specific surface area, morphological determinations, and FTIR analysis. The elemental analysis was performed using the Elemental Analyzer Flash 2000 (Thermo Scientific, Waltham, MA, USA), using the combustion method and the gas chromatographic method [26]. Heavy metal content was determined with NOVA A 300 Atomic Absorption Spectrophotometer (AAS) (Analytik Jena GmbH, Jena, Germany). The adsorbent materials were investigated via scanning electron microscopy with emission at a variable pressure. We used Field Emission Scanning Electron Microscope Variable Pressure—FESEM VP (CARL ZEISS, Oberkochen, Germany)—at a resolution of 0.8 nm at 30 kV and 2.5 nm at 30 kV in VP mode. We used the Brunauer–Emmett–Teller (BET) method for the measurement of the specific surfaces, and the analysis was performed using the Quantachrome Autosorb-IQ porosity equipment (Quantachrome Instruments, Boynton Beach, FL, USA).

The Fourier Transform Infrared Spectrometer Cary 630 ATR-FTIR (Agilent Technologies, Inc., Santa Clara, CA, USA) was used to determine the functional groups. The samples were first dried at 80 °C under vacuum conditions. The spectra were acquired with an attenuated total reflectance (ATR) module in the range 4000–400 cm<sup>-1</sup> (32 scans, 8 cm<sup>-1</sup> resolution, and 0.002 threshold).

## 2.3. CO<sub>2</sub> Adsorption Experiments

The adsorbent materials were tested in an experimental setup, shown in Figure 2, with the aim of assessing CO<sub>2</sub> removal and adsorption capacity.

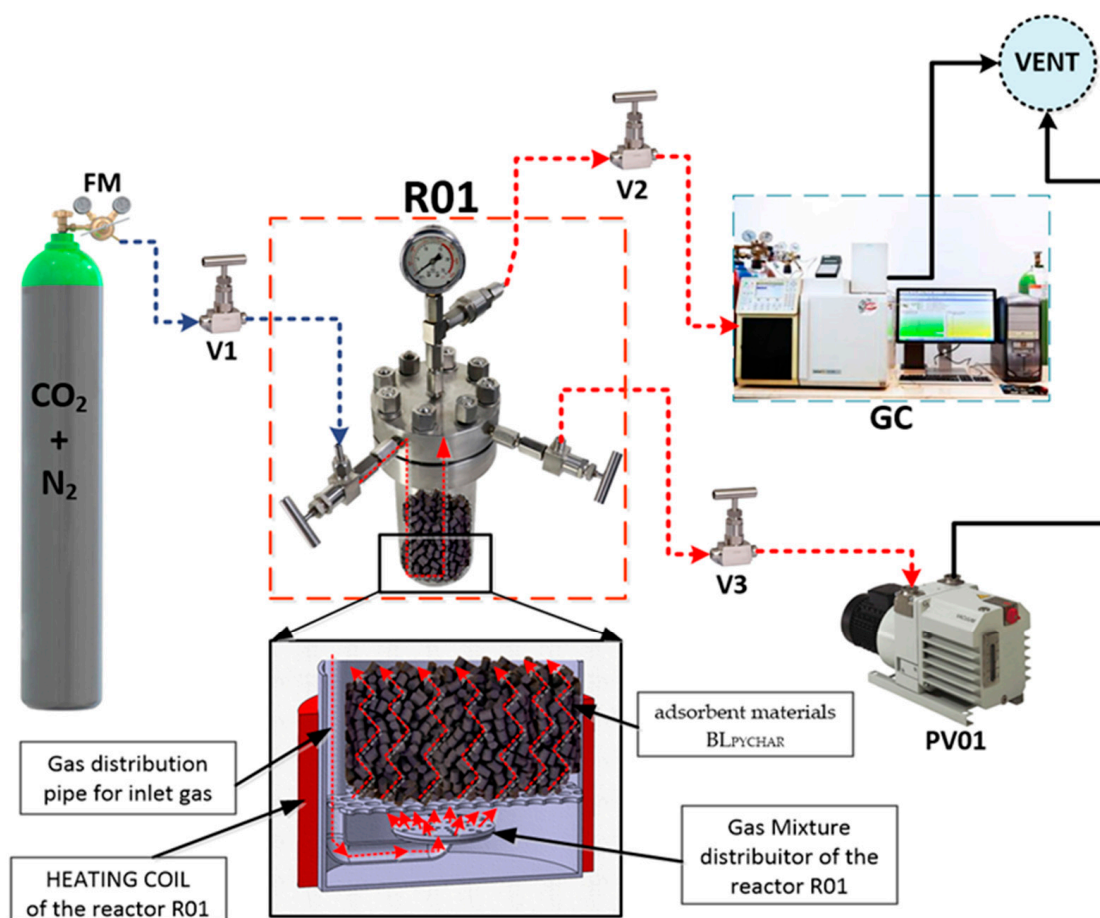


**Figure 2.** Flow sheet testing of adsorbent materials' levels of BLPYCHAR: CO<sub>2</sub> + N<sub>2</sub>—cylinder with test gas; FM—pressure and flow regulator; R01—reactor; V<sub>x</sub>—manual valve; GC—gas chromatograph; PV01—vacuum pump.

To test the effectiveness of the adsorbent materials, a binary gas with the composition of 81% CO<sub>2</sub> and 19% N<sub>2</sub> was prepared and used. A cartridge was used. The adsorbent materials were inserted in the form of pellets at an approximate weight of 1 g/pellet with a total mass of 200 g. In order to observe in real time when the adsorbents reached saturation, the test installation was connected to a gas chromatograph with a TCD detector (GC Varian CP 3800, Varian Inc., Palo Alto, CA, USA). The conditions of the adsorbent materials were as follows: ambient temperature, 5 psi pressure, and 100 mL/min gas flow rate. The adsorption capacity of CO<sub>2</sub>, the yield, and the degree of recovery of adsorbent materials were calculated using the following equations [33]:

$$a = \frac{Q \times p(C_i - C_f) \times t}{m} \quad (1)$$

where  $a$  = adsorption capacity, cm<sup>3</sup>/g;  $Q$  = the flow rate of the test gas passed over the adsorbent materials, cm<sup>3</sup>/s;  $p$  = adsorption pressure, bar;  $C_i$  = the initial CO<sub>2</sub> concentration, %vol;  $C_f$  = the final CO<sub>2</sub> concentration, %vol;  $t$  = time, s;  $m$  = adsorbent materials quantity from the reactor, g.

$$R_{CO_2} = \frac{C_e(CO_2) - C_i(CO_2)}{C_i(CO_2)} \times 100 \quad (2)$$

where  $R_{CO_2}$  = CO<sub>2</sub> recovery, %vol;  $C_e(CO_2)$  = average CO<sub>2</sub> concentrations up to the rupture period at the exit from adsorbent materials, %vol;  $C_i(CO_2)$  = initial CO<sub>2</sub> concentration, %vol.

$$\eta = \frac{C_a}{C_i} \times 100 \quad (3)$$

where  $\eta$  = separation efficiency, %;  $C_a$  = the concentration of adsorbed CO<sub>2</sub>, %;  $C_i$  = the concentration of initial CO<sub>2</sub>, %.

### 3. Results and Discussion

Table 2 shows the elemental composition of the adsorbent materials developed from the residue obtained after the BL pyrolysis. The elemental analysis showed that the C level contributed the most to the biochar composition, followed by S, H, and N. This was due to the BL content in terms of cellulose, hemicellulose, and lignin [34]. After the treatment with 5 M HCl, a notable increase in the concentrations of C and S was observed in the BL<sub>PYCHAR</sub> solid residues. Regarding the residue obtained following Cu-Zn-MCM-41 catalysis (group a), C and S concentrations reached 73.45% and 6.50%, respectively. Similarly, regarding the residue obtained from Ni-SBA-16 catalysis (group b), the C concentration rose to 77.04% and the S concentration rose to 6.21%. We also observed a decrease in the concentration of H after treatment with HCl, standing at 2.12% for 2a compared to the concentration seen for the BL<sub>PYCHAR</sub> (6.51%). The data were in correlation with other biochars after being subjected to deashing methods from the literature [35].

**Table 2.** Elemental composition of BL<sub>PYCHAR</sub> and resulted adsorbents.

Adsorbent Materials	H %	N %	S %	C %
BL <sub>PYCHAR</sub>	6.51	0.34	1.78	18.11
1a	0.93	0.22	2.10	34.96
1b	0.94	0.27	2.61	35.51
2a	2.12	0.47	6.50	73.45
2b	2.13	0.49	6.21	77.04
3a	1.87	0.29	1.04	36.62
3b	1.93	0.27	0.70	36.25
4a	1.17	0.30	0.96	37.06

After HCl treatment, the solid residues of both group a and group b suffered a decrease in metal content (Table 3), with levels between 18% (Cu) and 93% (Fe). A similar proportion was found for metals and elements in the second step of BL<sub>PYCHAR</sub> transformation. The exception was seen for the initial Cu concentrations, which was 1139.21 mg/kg in the case of sample 1a and around 67.26 mg/kg in the case of 1b. It was previously demonstrated that, after deashing with a HCl solution, the amounts of transitional metal, as well as the levels of P, significantly decreased. This was probably the explanation behind the increase in the concentration of C and S [35].

**Table 3.** Heavy metals extracted from adsorbent materials derived from BL<sub>PYCHAR</sub>.

Adsorbent Materials	Pb mg/kg	Cu mg/kg	Fe mg/kg	Ni mg/kg	Mn mg/kg	Zn mg/kg	Ca mg/kg	Mg mg/kg
1a	<6.00	1139.21	2145.26	16.55	36.21	374.89	424.57	383.39
1b	<6.01	67.26	2089.27	49.56	32.13	81.52	159.73	258.83
2a	<6.02	929.40	138.98	<3.00	<4.00	27.96	66.57	27.38
2b	<6.03	69.46	75.37	15.91	<4.01	7.22	55.73	8.57
3a	<6.04	741.33	788.78	<3.00	<4.02	51.39	68.66	51.32
3b	<6.05	41.67	647.03	16.29	<4.03	18.08	68.99	50.24
4a	<6.06	1101.89	985.00	<3.00	4.09	82.72	62.86	67.19

The SEM investigations (Figures 3 and 4) indicated that all the developed adsorbents had porous structures. It should also be noted that they had an aggregated morphology [36]. The differences observed between the samples were a consequence of the preparation method. These observations suggested that BL<sub>PYCHAR</sub>-based adsorbents have different types of functional groups that can play the binding role for CO<sub>2</sub> in different environments [37].

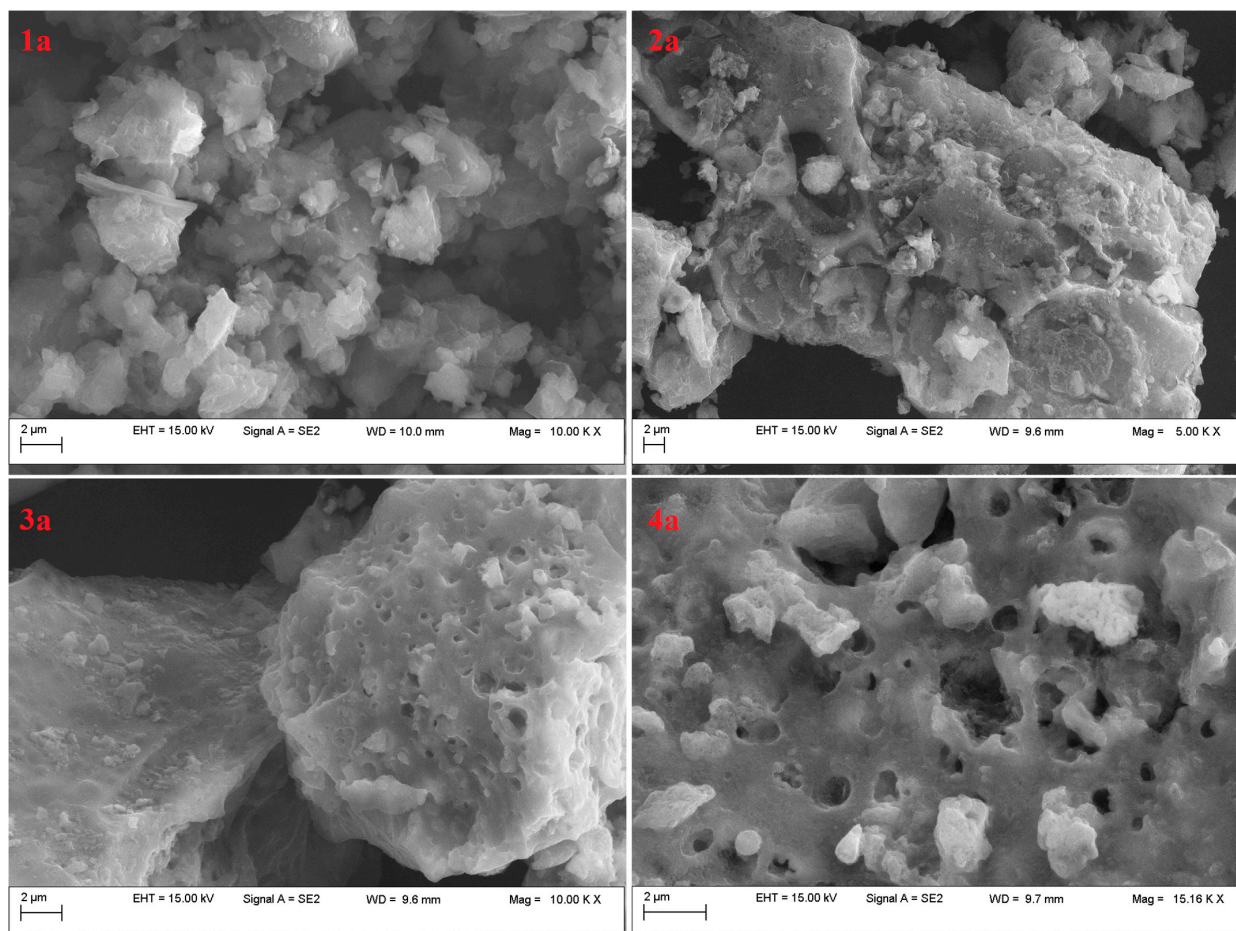


**Figure 3.** SEM images of the adsorbents resulted from BL<sub>PYCHAR</sub> (Cu-Zn-MCM-41-catalysed pyrolysis) (group a).

As for the calcined sample—4a, the grooves on the surface were destroyed, presenting a rougher surface (Figure 3(4a)). This was due to the decomposition of organic substances within the structure, and this was consistent with the literature [38].

After KOH treatment, clearer three-dimensional surface features were observed, results that were consistent with the literature (Figure 4) [39]. This may introduce the idea that these biochars should be more efficient in pollutant sequestration than HCl-based ones [36,37].

The surface chemistry and pore structure of the adsorbents essentially contribute to increasing the efficiency of the adsorption process.

N<sub>2</sub> adsorption–desorption isotherms are shown in Figure 5. The isotherms were classified as type II according to IUPAC as they were associated with a mesoporous structure, confirming the results obtained by the surface analysis. A mesoporous structure is highly beneficial for transporting CO<sub>2</sub> from a gaseous mixture to the adsorbent surface, which increases the adsorption capacity [40]. Therefore, many functional groups from this type of material can provide effective active centres at the solid–gas surface interface, granting higher adsorption capacities in terms of CO<sub>2</sub>.

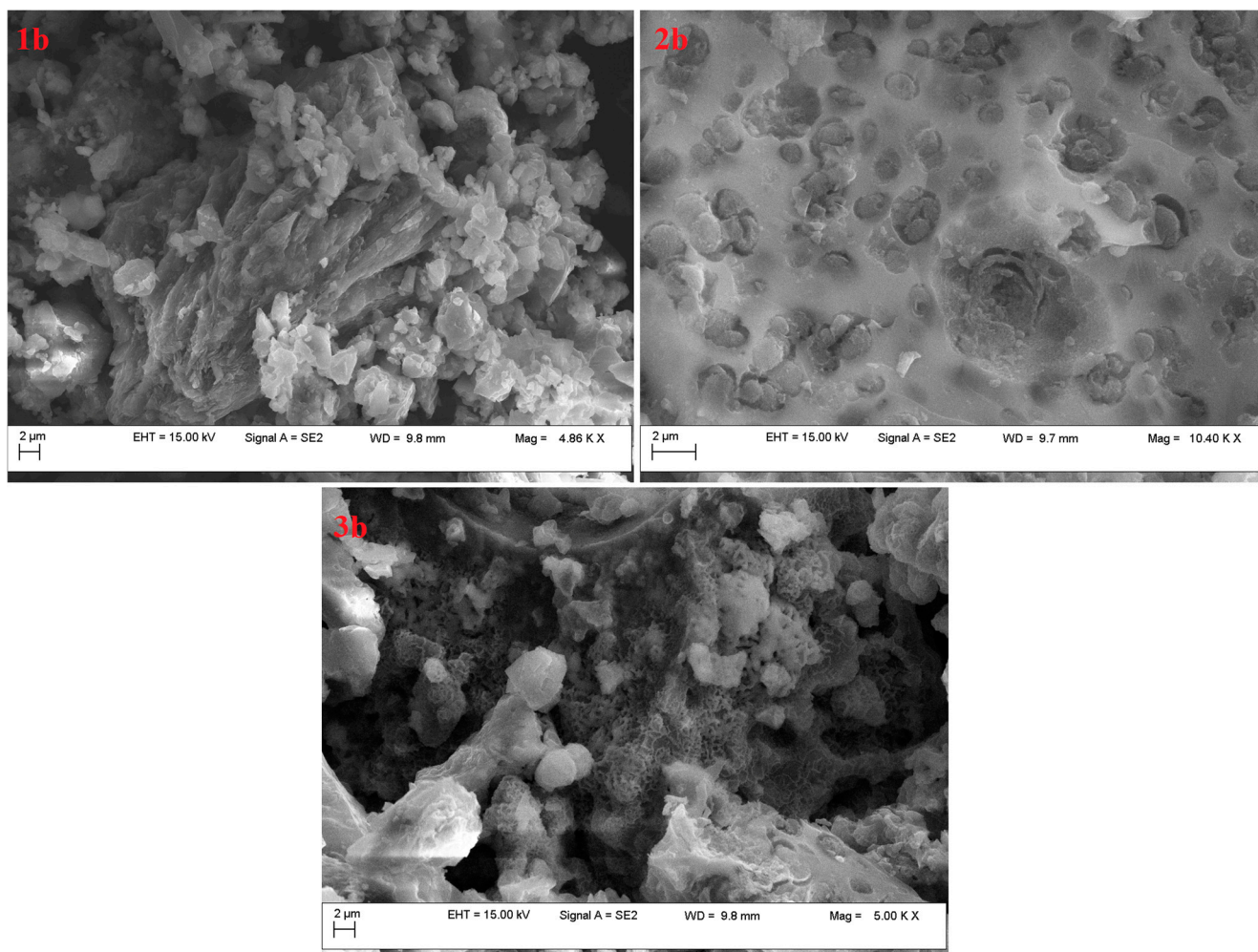


**Figure 4.** SEM images of the adsorbents taken from BL<sub>PYCHAR</sub> (Ni-SBA-16-catalysed pyrolysis) (group b).

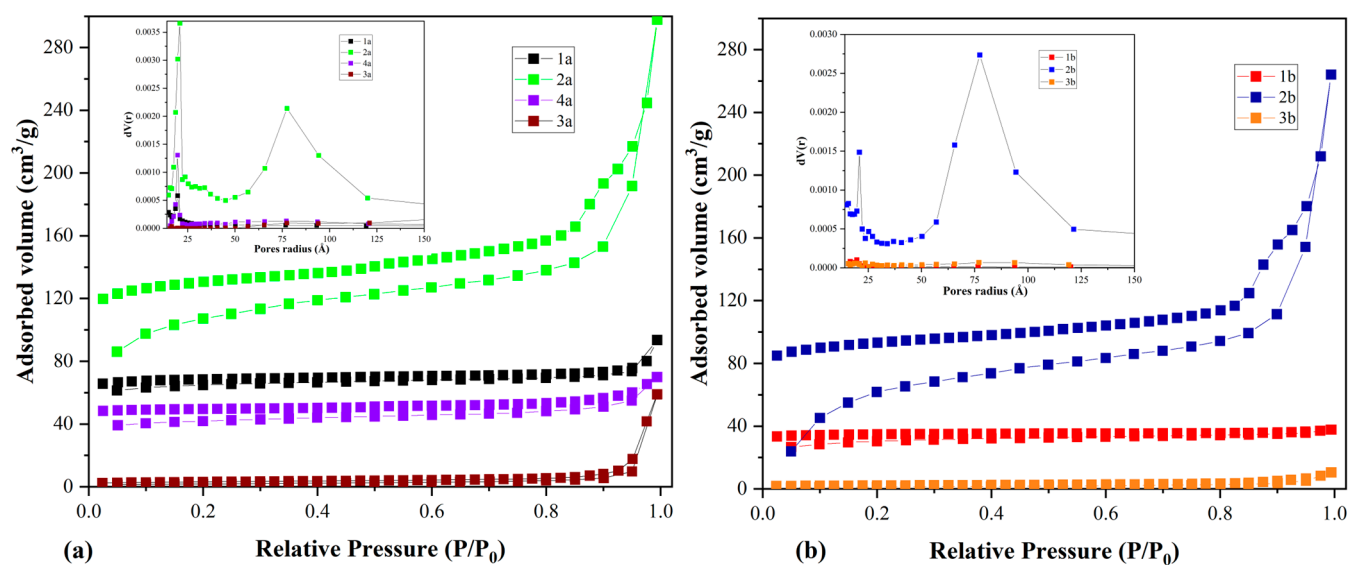


**Figure 5.** Adsorption isotherms and pore distribution of the BL<sub>PYCHAR</sub>-derived materials: (a) adsorbent—group a; (b) adsorbent—group b.



Specific surface area and microporosity are interconnected; the creation of numerous small micropores leads to an increased specific surface area. This larger surface area offers more active sites for CO<sub>2</sub> adsorption via physical adsorption [41].

Analysing the samples obtained after HCl treatment, the highest specific surface area was reported for the sample 1a, 75.37 m<sup>2</sup>/g, although lignocellulosic biochars generally have low surface areas due to the nature of cellulose and hemicellulose (Table 4) [42]. BET investigations indicate that the sample 2b had a higher specific surface than the initial biochar, standing at 224.06 m<sup>2</sup>/g versus 54.29 m<sup>2</sup>/g, which was superior by comparison to the adsorbent 2a (Table 4).

**Table 4.** Textural properties of adsorbent materials derived from BL<sub>PYCHAR</sub>.

Adsorbent Materials	S <sub>BET</sub> m <sup>2</sup> /g	V cm <sup>3</sup> /g	D <sub>V</sub> (τ) Å
1a	75.37	0.04	19.68
2a	54.47	0.28	20.86
3a	6.36	0.09	303.78
4a	41.34	0.03	19.66
1b	54.29	0.01	19.65
2b	224.06	0.28	77.41
3b	4.33	0.01	76.98

For all the obtained adsorbents, the pore volume was low. This is an attribute of the initial structure of cellulose, lignocellulose, and lignin, which are characterized by small amounts of pores or even blocked pores [43]. In addition, the materials showed small pore diameters, between 1.96 nm and 7.7 nm, indicating that these materials are mesoporous and may be suitable for use as adsorbents in the gas phase as they facilitate the diffusion of adsorbates into adsorbent structures. An interesting case was the sample 3a, which exhibited a higher pore diameter, around 30.3 nm, at the upper limit of the mesoporous interval at the same time as a drastic decrease in specific surface area. This was also in accordance with the morphology revealed via SEM (agglomerated particles and smoother surface).

The adsorbent 2b stood out among all materials. It had an irregular morphology, as SEM investigation revealed (Figure 4(2b)), pore diameters of around 7.7 nm, and the highest surface area (224 m<sup>2</sup>/g), which represents an advantage in CO<sub>2</sub> adsorption. As the isotherms showed, sample 2b showed a higher level of adsorption, with the pore volume reaching 0.28 cm<sup>3</sup>/g.

These findings were mainly correlated with the inorganic minerals blocking the pores of BL-based adsorbents being washed away, resulting in more exposed pores and improving the characteristics of the porous structure [35]. Moreover, inorganic minerals may obstruct direct contact between potassium hydroxide and the carbon skeleton to some extent, thus, potassium hydroxide can interact directly with the carbon structure, resulting in more efficient etching. The impact of potassium hydroxide activation becomes particularly noticeable after deashing with HCl. As a result, the specific surface area and micropore area of sample 2b were higher [35].

Earlier research indicated that adsorbents with a large surface area can exhibit a high capacity for CO<sub>2</sub> capture. For example, when coffee grounds were used to produce biochar, the successful capture of CO<sub>2</sub> was achieved at temperatures between 30 and 90 °C under a constant CO<sub>2</sub> concentration, with a maximum adsorption capacity of 2.8 mmol/g at a BET surface area of 539 m<sup>2</sup>/g for the biochar [44].

Figure 6 and Table 5 present the FTIR spectra and peak assignment. For reasons of comparison, the black liquor (BL) spectrum was also introduced. Peaks with values below 1000 cm<sup>-1</sup> characterized the deformation vibrations of the CH bonds associated with aromatic rings, while the absorption band around the value of 3340 cm<sup>-1</sup> corresponded to the OH stretching vibration, indicating the presence of phenols, alcohols, or carboxylic

acids in BL [45]. Also, the presence of a significant peak at  $2329\text{ cm}^{-1}$  (representing the stretching vibration of the C-H bond in the methyl and methylene groups) was found. The peak at  $1643\text{ cm}^{-1}$  indicated the vibrations of the aromatic backbone plus the C=O stretching vibration [45–49].

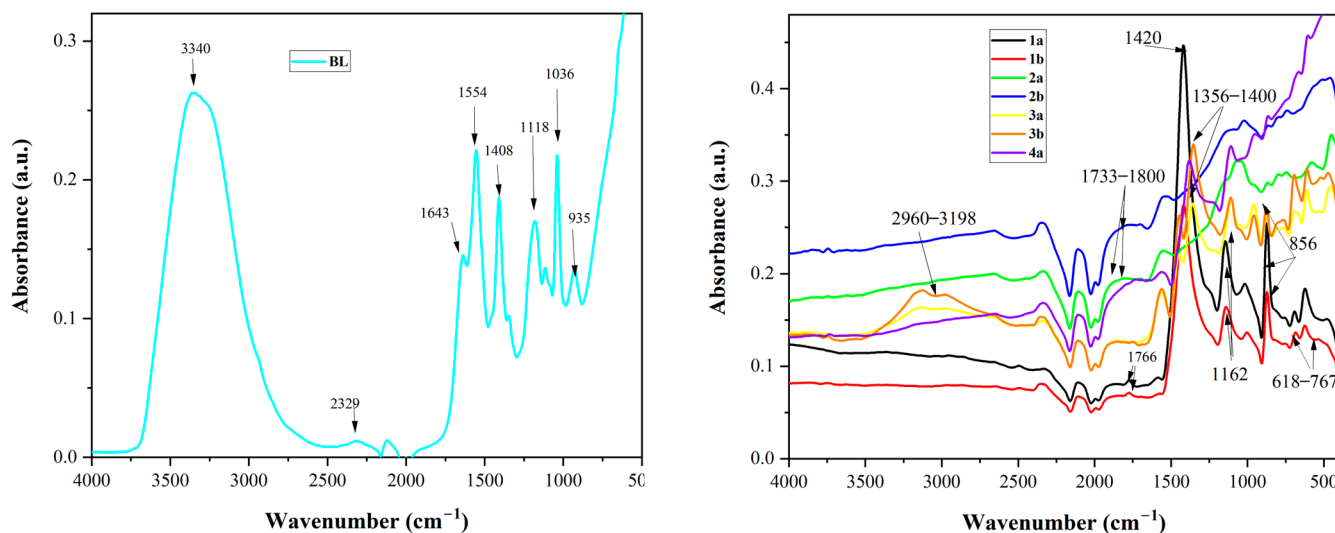


**Figure 6.** FT-IR spectra of BL (left) and the adsorbent materials derived from BL<sub>PYCHAR</sub> (right).

**Table 5.** Peaks and bands identified in the BL spectrum.

Wavenumber ( $\text{cm}^{-1}$ )	Assignment
935	C-H out of plan
1036–1118	C-O deformation from primary alcohols
1185	C-O vibration plus C=O and C-C from guaianyl and syringyl cores
1408	in-plane deformation of OH
1554	C-H vibration
1643	The vibration of the aromatic nucleus plus the C=O stretch
2329	C-H stretching from methyl and methylene groups
3340	O-H stretching from phenols, alcohols, and water

Compared to the FTIR spectrum of BL, the absorption peaks for BL<sub>CHAR</sub> resulting from pyrolysis were much simpler. The band at  $3340\text{ cm}^{-1}$ , characterizing the -OH stretching vibration, disappeared after pyrolysis. This indicated the removal of alcohol groups from branched chains by pyrolysis (not phenols and carboxylic acids, as they mostly existed as phenolates and carboxylates in BL) [30]. The evolution of the peaks at about  $1554$  and  $1643\text{ cm}^{-1}$  clearly indicated that the carbonyl and/or carboxyl groups were removed by pyrolysis. The removal was complete at temperatures above  $450\text{ }^{\circ}\text{C}$ . The peaks at  $1420\text{ cm}^{-1}$  and  $856\text{ cm}^{-1}$  were characteristic of absorptions due to potassium carbonate, revealing that its content increased upon treatment with potassium hydroxide [50]. The peaks of about  $1162\text{ cm}^{-1}$  were assigned to the remaining C-O-C stretching of ester groups in cellulose and hemicellulose [51]. The three-peak group at  $618\text{--}767\text{ cm}^{-1}$  in the FTIR spectra was attributed to residual aromatic C-H bands [51].

The peaks of KOH-activated adsorbent materials were stronger, indicating that the abundance of surface functional group species was higher. For example, the peak at  $1766\text{ cm}^{-1}$  in the sample 1a, attributed to the C=O vibration, underwent a shift and transformation into a broad band in the activated materials at about  $1733\text{--}1800\text{ cm}^{-1}$ , indicating the intense presence of these groups on the surface. Also, the peaks at  $1356\text{--}1400\text{ cm}^{-1}$  were assigned, as in the case of the starting material, to the C-H stretching vibrations of the  $\text{CH}_2$  and  $\text{CH}_3$  groups. The intensity of these peaks for the activated materials highlighted the increased rate

of distribution of OH and CH<sub>2</sub> structures. The biochar spectra of sample 3b showed alkyl bands around 2960 and 3198 cm<sup>-1</sup>, which were correlated with the hydrophobicity index of the remaining BL organic matter [51].

Table 6 represents the results obtained after testing the adsorbent material 2b, displaying the number of injections, the duration of the adsorption process, the evolution of CO<sub>2</sub>, the adsorption capacity of CO<sub>2</sub>, the yield, and the degree of recovery of these adsorbent materials. From all adsorbent materials, the sample 2b (2b—BL<sub>PYCHAR\_Ni-SBA-16\_HCl</sub>) was chosen because of its high specific surface area (224.06 m<sup>2</sup>/g) and pore volume (0.28 cm<sup>3</sup>/g) and its medium diameter (7.7 nm). For comparison, the sample 3b (BL<sub>PYCHAR\_Ni-SBA-16\_HCl+KOH</sub> (1:1)), with the lowest specific surface area (4.33 m<sup>2</sup>/g) and pore volume (0.01 cm<sup>3</sup>/g), was tested.

**Table 6.** CO<sub>2</sub> adsorption evolution and efficiency.

Gas Mixture	Injection	CO <sub>2</sub> Evolution vol%		Adsorption Capacity cm <sup>3</sup> /g		Separation Efficiency %		Recovery %	
		3b	2b	3b	2b	3b	2b	3b	2b
81 vol% CO <sub>2</sub> balance N <sub>2</sub>	1	69.22	69.32						
	2	69.01	58.13						
	3	67.33	49.77						
	4	62.47	40.12						
	5	60.66	31.03						
	6	59.05	22.75	17.59	18.57	94.52	99.78	40.45	62.98
	7	42.44	15.47						
	8	29.91	9.33						
	9	17.81	3.78						
	10	4.44	0.18						

As can be seen in Table 6, the adsorption capacity of the adsorbent materials was tested on a mixture of gases. The saturation of the adsorbent materials could be assessed after 10 injections. The injection duration was 80 s, and the recovery of the CO<sub>2</sub> concentration from the adsorbent materials was carried out using a vacuum pump at a pressure of 10<sup>-2</sup> bar. The final adsorption capacity for sample 2b reached 18.57 cm<sup>3</sup>/g. The efficiency of the CO<sub>2</sub> separation process from the gas mixture was 99.78% and the yield of the CO<sub>2</sub> recovery process from the adsorbent materials was 62.98%. It was observed that, for the sample with the lowest specific surface area, which was 3b, the final adsorption capacity reached 17.59 cm<sup>3</sup>/g. In this process, the efficiency of the CO<sub>2</sub> separation process from the gas mixture was 94.52% and the yield of the CO<sub>2</sub> recovery process from the adsorbent materials was 40.45%. Although the difference between the adsorption capacity of the two samples was not very high, an increased recovery percentage was observed in the case of the sample with the highest surface area.

It can be stated that the CO<sub>2</sub> adsorption process depended on parameters such as pressure and the adsorbent's specific surface area. The tested adsorbent material, 2b, had a high specific surface area, showing a higher adsorption capacity (18.57 cm<sup>3</sup>/g) than a commercial adsorbent (activated carbon). It had a higher specific surface area (1470 m<sup>2</sup>/g), but a lower adsorption capacity, which started from 0.2 mmol/g (about 4.48 cm<sup>3</sup>/g) [52].

Various authors studied the impact of temperatures [53]. Temperature significantly affects the CO<sub>2</sub> adsorption capacity, which is crucial for its capture following combustion. It was stated that the chosen temperature influenced the type of adsorption that took place, whether it was physisorption or chemisorption [53]. For example, at 30 °C, the adsorption capacity of commercial activated carbons reached 0.68 mmol CO<sub>2</sub>/g (about 15.23 cm<sup>3</sup>/g) adsorbent. The observed overall trend was that CO<sub>2</sub> adsorption declined as temperature increased, falling to 0.17 mmol CO<sub>2</sub>/g (about 3.80 cm<sup>3</sup>/g) adsorbent at 70 °C [53]. These findings, together with the experimental results highlighted within the present study, align with the literature, which indicates that gas adsorption diminishes with increasing temperature [53]. As temperature increases at a constant flow rate, the kinetic energy of the gases also rises, resulting in reduced surface coverage of CO<sub>2</sub>. This pattern can be attributed to the exothermic nature of the

adsorption process. Another parameter that can influence the adsorption capacity is the flow rate. The literature mentions that, in the case of using commercial activated carbons, the highest CO<sub>2</sub> adsorption was observed at a flow rate of 30 mL/min and 30 °C [53]. Adsorption at flow rates up to 70 mL/min (30 °C—0.40 mmol CO<sub>2</sub>/g adsorbent and 70 °C—0.17 mmol CO<sub>2</sub>/g adsorbent) was lower than that achieved at 30 mL/min (30 °C—0.68 mmol CO<sub>2</sub>/g adsorbent and 70 °C—0.06 mmol CO<sub>2</sub>/g adsorbent) [53]. Reducing the gas inlet flow rate has been shown to increase contact time and enhance mass transfer between CO<sub>2</sub> and the adsorbents. The motivation was that lower flow rates improved the retention time of CO<sub>2</sub> molecules on the selected adsorbents within the packed bed adsorption column, leading to a higher amount of CO<sub>2</sub> being adsorbed. At lower flow rates, the adsorbate (CO<sub>2</sub>) has more time to interact with the adsorbent, resulting in higher CO<sub>2</sub> adsorption capacity [54].

It was demonstrated that activated carbon with a higher surface area had an improved performance in terms of CO<sub>2</sub> adsorption. However, some studies revealed that sugar cane-derived activated carbon exhibited improved adsorption sites compared to kaolinite or activated carbon–kaolinite composites at a temperature of 30 °C [53]. The kaolinite–activated carbon composite revealed an adsorption capacity of 0.42 mmol CO<sub>2</sub>/g (9.40 cm<sup>3</sup>/g), while kaolinite had the lowest capacity at 0.29 mmol CO<sub>2</sub>/g (6.49 cm<sup>3</sup>/g) [53]. The enhanced CO<sub>2</sub> adsorption capacity of the activated carbon materials at low flow rates suggests an improved affinity for CO<sub>2</sub> due to the presence of activated carbon.

As was previously demonstrated, the amount of adsorbed CO<sub>2</sub> showed a nearly linear increase with rising surface area, suggesting that this is a key factor affecting adsorption performance [55]. Also, no clear correlation was found between the volume of other pores and CO<sub>2</sub> adsorption. In contrast, a relatively strong positive correlation was observed between micropore volume and CO<sub>2</sub> adsorption [55]. These results indicated that the CO<sub>2</sub> adsorption efficiency of a biochar may be primarily influenced by micropore size. The correlation between total pore volume and CO<sub>2</sub> adsorption can be linked to the relationship between micropore volume and CO<sub>2</sub> uptake [55].

Thus, it can be concluded that the development of micropores significantly impacts CO<sub>2</sub> adsorption capacity. Consequently, it can be stated that surface area and micropore volume can serve as guidelines for obtaining materials with high CO<sub>2</sub> adsorption characteristics.

#### 4. Conclusions

Following the pyrolysis process of black liquor, under different experimental conditions, a solid BL<sub>PYCHAR</sub> residue was obtained, which was further transformed into CO<sub>2</sub>-adsorbent materials. Seven types of adsorbent materials were developed, exhibiting relatively high specific surfaces and different pore diameters. The most efficient adsorbent material was 2b—BL<sub>PYCHAR</sub><sub>Ni-SBA-16</sub>\_HCl, which had the highest specific surface area of 224.06 m<sup>2</sup>/g, the highest pore volume of 0.28 cm<sup>3</sup>/g, and the highest pore diameter of around 7.7 nm compared to the other adsorbent materials treated with KOH, which had lower values. To test the efficiency of the 2b—BL<sub>PYCHAR</sub><sub>Ni-SBA-16</sub>\_HCl, a CO<sub>2</sub> adsorption testing setup was used. The BL<sub>PYCHAR</sub><sub>Ni-SBA-16</sub>\_HCl adsorbent was tested on a gas mixture with a concentration of 81% CO<sub>2</sub> and 19% N<sub>2</sub>, with saturation occurring after 10 injections. The adsorption capacity of the adsorbent material with the highest specific surface area was 18.57 cm<sup>3</sup>/g. It also had a separation efficiency of 99.78% and a recovery degree of 62.98%. The sample with the lowest specific surface area registered a final adsorption capacity of 17.59 cm<sup>3</sup>/g, with an efficiency of 94.52% and a recovery of 40.45%. Although the difference between the adsorption capacity of the two samples was not so high, an increased recovery percent was observed in the case of the sample with the highest surface area. Therefore, the obtained material could be used as a potential candidate for CO<sub>2</sub> capture and storage even at high concentrations. As a general conclusion, it can be stated that biochar resulting from waste valorisation is a promising candidate for CO<sub>2</sub> capture materials, reducing anthropogenic CO<sub>2</sub> emission and mitigating global warming. Although advancements were

made in biochar obtention, more research is needed to produce adsorbents with increased adsorption capacity and long-term stability for scaling CO<sub>2</sub> capture.

**Author Contributions:** Conceptualization, A.M.Z., S.I.S., F.M. and S.O.; data curation, A.M.Z., V.-C.N. and S.O.; formal analysis, A.M.Z., V.-C.N., C.S., S.I.S., A.S. and F.M.; funding acquisition, V.-C.N.; investigation, A.M.Z., V.-C.N., C.S., A.S. and F.M.; methodology, A.M.Z., V.-C.N., C.S., S.I.S., A.S. and F.M.; project administration, V.-C.N.; resources, S.O.; software, V.-C.N. and S.I.S.; supervision, V.-C.N. and S.O.; validation, V.-C.N. and S.O.; visualization, V.-C.N. and S.O.; writing—original draft, A.M.Z., V.-C.N. and F.M.; writing—review and editing, V.-C.N. and S.O. All authors have read and agreed to the published version of the manuscript.

**Funding:** The work has been funded by the Romanian Ministry of Research Innovation and Digitalization, under NUCLEU Program-Financing Contract no. 20N/05.01.2023, Project PN 23 15 04 02: “Laboratory experiments valorisation in the development of technologies for the production of biofuels from agro-industrial waste”.

**Institutional Review Board Statement:** Not applicable.

**Informed Consent Statement:** Not applicable.

**Data Availability Statement:** Data are contained within the article.

**Acknowledgments:** The authors are grateful to Adriana Marinouiu (ICSI Energy Department), from National Research and Development Institute for Cryogenic and Isotopic Technologies—ICSI Ramnicu Valcea, for specific surface area and pores distribution determination.

**Conflicts of Interest:** The authors declare no conflicts of interest.

## References

1. Zhao, J.; Zhang, W.; Shen, D.; Zhang, H.; Wang, Z. Preparation of porous carbon materials from black liquor lignin and its utilization as CO<sub>2</sub> adsorbents. *J. Energy Inst.* **2023**, *107*, 101179. [[CrossRef](#)]
2. Ramonet, M.; Chatterjee, A.; Ciais, P.; Levin, I.; Sha, M.K.; Steinbacher, M.; Sweeney, C. *CO<sub>2</sub> in the Atmosphere: Growth and Trends Since 1850*; OREs: New York, NY, USA, 2023.
3. Zhang, X.G.; Buthiyappan, A.; Jewaratnam, J.; Metselaar, H.S.C.; Raman, A.A.A. Bifunctional materials for integrated CO<sub>2</sub> capture and conversion: Review on adsorbent and catalyst types, recent advances, and challenges. *J. Environ. Chem. Eng.* **2023**, *12*, 111799. [[CrossRef](#)]
4. Kong, M.; Song, L.; Liao, H.; Zhang, S.; Wang, Y.; Deng, X.; Feng, W. A review on development of post-combustion CO<sub>2</sub> capture technologies: Performance of carbon-based, zeolites and MOFs adsorbents. *Fuel* **2024**, *371*, 132103. [[CrossRef](#)]
5. Davoodi, S.; Al-Shargabi, M.; Wood, D.A.; Rukavishnikov, V.S.; Minaev, K.M. Review of technological progress in carbon dioxide capture, storage, and utilization. *Gas Sci. Eng.* **2023**, *117*, 205070. [[CrossRef](#)]
6. Hurlbert, M.; Osazuwa-Peters, M. Carbon capture and storage in Saskatchewan: An analysis of communicative practices in a contested technology. *Renew. Sustain. Energy Rev.* **2023**, *173*, 113104. [[CrossRef](#)]
7. Rogelj, J.; Huppmann, D.; Krey, V.; Riahi, K.; Clarke, L.; Gidden, M.; Meinshausen, M. A new scenario logic for the Paris Agreement long-term temperature goal. *Nature* **2019**, *573*, 357–363. [[CrossRef](#)]
8. Gul, A.; Un, U.T. Effect of temperature and gas flow rate on CO<sub>2</sub> capture. *Eur. J. Sustain. Dev. Res.* **2022**, *6*, em0181. [[CrossRef](#)]
9. Udrouiu, N.A.; Nicolae, C.G. Possibilities to reduce CO<sub>2</sub> emissions by using electric motors with high energy efficiency. *Sci. Pap. Ser.* **2022**, *65*, 428–435.
10. Zhu, Q. Developments on CO<sub>2</sub>-utilization technologies, *Clean. Energy* **2019**, *3*, 85–100.
11. Duyar, D.S.; Trevino, M.A.A.; Farrauto, R.J. Dual function materials for CO<sub>2</sub> capture and conversion using renewable H<sub>2</sub>. *Appl. Catal. B Environ.* **2015**, *168*, 370–376. [[CrossRef](#)]
12. Zongze, L.V.; Changlei, Q.; Shuzhen, C.; Dawid, P.; Hanak, C.W. Efficient-and-stable CH<sub>4</sub> reforming with integrated CO<sub>2</sub> capture and utilization using Li<sub>4</sub>SiO<sub>4</sub> sorbent. *Sep. Purif. Technol.* **2021**, *277*, 119476.
13. Wang, G.; Guo, Y.; Yu, J.; Liu, F.; Sun, J.; Wang, X.; Wang, T.; Zhao, C. Ni-CaO dual function materials prepared by different synthetic modes for integrated CO<sub>2</sub> capture and conversion. *Chem. Eng. J.* **2022**, *428*, 132110. [[CrossRef](#)]
14. Oliveira, M.; Santos, V.G.; Carvalho, L.S.; Ruiz, D.; Barbosa, I.A.S.; das Virgens, C.F.; Martins, A.R. Adsorbentes obtidos de resíduos de licor negro: Síntese, caracterização e avaliação na remoção de corantes têxteis. *Sci. Plena* **2020**, *16*, 1–11. [[CrossRef](#)]
15. Miricioiu, M.G.; Zaharioiu, A.; Oancea, S.; Bucura, F.; Raboaca, M.S.; Filote, C.; Ionete, R.E.; Niculescu, V.C.; Constantinescu, M. Sewage Sludge Derived Materials for CO<sub>2</sub> Adsorption. *Appl. Sci.* **2021**, *11*, 7139. [[CrossRef](#)]
16. Zaharioiu, A.M.; Şandru, C.; Ionete, E.I.; Marin, F.; Ionete, R.E.; Soare, A.; Constantinescu, M.; Bucura, F.; Niculescu, V.-C. Eco-Friendly Alternative Disposal through the Pyrolysis Process of Meat and Bone Meal. *J. Mater.* **2022**, *15*, 6593. [[CrossRef](#)] [[PubMed](#)]

17. Liu, X.; Shen, F.; Smith, R.L.; Qi, X. Black liquor-derived calcium-activated biochar for recovery of phosphate from aqueous solutions. *Bioresour. Technol.* **2019**, *294*, 122198. [[CrossRef](#)]
18. Sari, A.A.; Amriani, F.; Muryanto, M.; Triwulandari, E.; Sudiyani, Y.; Barlianti, V. Mechanism, adsorption kinetics and applications of carbonaceous adsorbents derived from black liquor sludge. *J. Taiwan Inst. Chem. Eng.* **2017**, *77*, 236–243. [[CrossRef](#)]
19. Kelm, M.A.P.; da Silva Júnior, M.J.; de Barros Holanda, S.H.; de Araujo, C.M.B.; de Assis Filho, R.B.; Freitas, E.J. Removal of azo dye from water via adsorption on biochar produced by the gasification of wood wastes. *Environ. Sci. Pollut. Res.* **2019**, *26*, 28558–28573. [[CrossRef](#)]
20. Cardoso, M.; Gonçalves, C.R.S.; Oliveira, É.D.; Passos, M.L.A. *Caracterização do Licor Negro de Eucalipto Proveniente da Indústria de Papel*; Congreso Iberoamericano de Investigación en Celulose y Papel: Iguazú, Argentina, 2000.
21. Antonakou, E.; Lappas, A.; Merete, H.N.; Aud, B.; Stöcker, M. Evaluation of various types of Al-MCM-41 materials as catalysts in biomass pyrolysis for the production of bio-fuels and chemicals. *Fuel* **2006**, *85*, 2202–2212. [[CrossRef](#)]
22. Chen, J.; Liu, C.; Wu, S.; Liang, J.; Lei, M. Enhancing the quality of bio-oil from catalytic pyrolysis of kraft black liquor lignin. *RSC Adv.* **2016**, *6*, 107970–107976. [[CrossRef](#)]
23. Jeon, M.-J.; Jeon, J.-K.; Suh, D.J.; Park, S.H.; Sa, Y.J.; Joo, S.H.; Park, Y.-K. Catalytic pyrolysis of biomass components over mesoporous catalysts using Py-GC/MS. *Catal. Today* **2013**, *204*, 170–178. [[CrossRef](#)]
24. Beck, J.S.; Vartuli, J.C.; Roth, W.J.; Leonowicz, M.E.; Kresge, C.T.; Schmitt, K.D.; Chu, C.T.W.; Olson, D.H.; Sheppard, E.W.; McCullen, S.B.; et al. A new family of mesoporous molecular sieves prepared with liquid crystal templates. *J. Am. Chem. Soc.* **1992**, *114*, 10834–10843. [[CrossRef](#)]
25. Marin, F.; Bucura, F.; Niculescu, V.-C.; Roman, A.; Botoran, O.R.; Constantinescu, M.; Spiridon, S.I.; Ionete, E.I.; Oancea, S.; Zaharioiu, A.M. Mesoporous Silica Nanocatalyst-Based Pyrolysis of a By-Product of Paper Manufacturing, Black Liquor. *Sustainability* **2024**, *16*, 3429. [[CrossRef](#)]
26. Kiani, P.; Meshksar, M.; Rahimpour, M.R. Biogas reforming over La-promoted Ni/SBA-16 catalyst for syngas production: Catalytic structure and process activity investigation. *Int. J. Hydrog. Energy* **2023**, *48*, 6262–6274. [[CrossRef](#)]
27. Sun, C.; Summa, P.; Wang, Y.; Świrk Da Costa, K.; Miró i Rovira, A.; Casale, S.; Świerczek, K.; Hu, C.; Rønning, M.; Da Costa, P. Boosting CO<sub>2</sub> reforming of methane via the metal-support interaction in mesostructured SBA-16-derived Ni nanoparticles. *Appl. Mater. Today* **2022**, *26*, 101354. [[CrossRef](#)]
28. Shi, Y.; Liu, C.; Zhuo, J.; Yao, Q. Investigation of a Ni-Modified MCM-41 Catalyst for the Reduction of Oxygenates and Carbon Deposits during the Co-Pyrolysis of Cellulose and Polypropylene. *ACS Omega* **2020**, *5*, 20299–20310. [[CrossRef](#)]
29. Karnjanakom, S.; Guan, G.; Asep, B.; Hao, X.; Kongparakul, S.; Samart, C.; Abudula, A. Catalytic Upgrading of Bio-Oil over Cu/MCM-41 and Cu/KIT-6 Prepared by β-Cyclodextrin-Assisted Coimpregnation Method. *J. Phys. Chem. C* **2016**, *120*, 3396–3407. [[CrossRef](#)]
30. Al-Kaabi, Z.; Pradhan, R.; Thevathasan, N.; Gordon, A.; Chiang, Y.W.; Dutta, A. Bio-carbon production by oxidation and hydrothermal carbonization of paper recycling black liquor. *J. Clean. Prod.* **2019**, *213*, 332–341. [[CrossRef](#)]
31. Boucard, H.; Weiss-Hortala, E.; Gueye, F.; Espitalier, F.; Barna, R. Insights in mechanisms of carbonaceous microparticles formation from black liquor hydrothermal conversion. *J. Supercrit. Fluids* **2020**, *161*, 104817. [[CrossRef](#)]
32. Zhang, J.P.; Sun, Y.; Woo, M.W.; Zhang, L.; Xu, K.Z. Preparation of steam activated carbon from black liquor by flue gas precipitation and its performance in hydrogen sulfide removal: Experimental and simulation works. *J. Taiwan Inst. Chem. Eng.* **2016**, *59*, 395–404. [[CrossRef](#)]
33. Sethupathi, S.; Zhang, M.; Upamali Rajapaksha, A.; Lee, S.R.; Nor, N.M.; Mohamed, A.R.; Al-Wabel, M.; Lee, S.S.; Ok, Y.S. Biochars as Potential Adsorbers of CH<sub>4</sub>, CO<sub>2</sub> and H<sub>2</sub>S. *Sustainability* **2017**, *9*, 121. [[CrossRef](#)]
34. Morya, R.; Kumar, M.; Tyagi, I.; Pandey, A.K.; Park, J.; Raj, T.; Sirohi, R.; Kumar, V.; Kim, S.-H. Recent advances in black liquor valorization. *Bioresour. Technol.* **2022**, *350*, 126916. [[CrossRef](#)]
35. Zhang, J.; Shao, J.; Jin, Q.; Zhang, X.; Yang, H.; Chen, Y.; Zhang, S.; Chen, H. Effect of deashing on activation process and lead adsorption capacities of sludge-based biochar. *Sci. Total Environ.* **2020**, *716*, 137016. [[CrossRef](#)]
36. Suman, S.; Panwar, D.S.; Gautam, S. Surface morphology properties of biochars obtained from different biomass waste. *Energy Sources Part A Recovery Util. Environ. Eff.* **2017**, *39*, 1007–1012. [[CrossRef](#)]
37. Huang, H.; Reddy, N.G.; Huang, X.; Chen, P.; Wang, P.; Zhang, Y.; Huang, Y.; Lin, P.; Garg, A. Effects of pyrolysis temperature, feedstock type and compaction on water retention of biochar amended soil. *Sci. Rep.* **2021**, *11*, 7419. [[CrossRef](#)]
38. Li, S.Y.; Teng, H.-J.; Guo, J.-Z.; Wang, Y.-X.; Li, B. Enhanced removal of Cr(VI) by nitrogen-doped hydrochar prepared from bamboo and ammonium chloride. *Bioresour. Technol.* **2021**, *342*, 126028. [[CrossRef](#)]
39. Rwiza, M.J.; Kleinke, M.; Kim, K.W. A study on Pb removal kinetics using modified agricultural wastes from Tanzania. *SN Appl. Sci.* **2020**, *2*, 1921. [[CrossRef](#)]
40. Petrovic, B.; Gorbounov, M.; Soltani, S.M. Influence of surface modification on selective CO<sub>2</sub> adsorption: A technical review on mechanisms and methods. *Microporous Mesoporous Mater.* **2021**, *312*, 110751. [[CrossRef](#)]
41. Guo, S.; Li, Y.; Wang, Y.; Wang, L.; Sun, Y.; Liu, L. Recent advances in biochar-based adsorbents for CO<sub>2</sub> capture. *Carbon Capture Sci. Technol.* **2022**, *4*, 100059. [[CrossRef](#)]
42. Kumar, V.; Sharma, N.; Panneerselvam, B.; Kumar, L.; Huligowda, D.; Umesh, M.; Gupta, M.; Muzammil, K.; Zahrani, Y.; Malmuthheibi, M. Lignocellulosic biomass for biochar production: A green initiative on biowaste conversion for pharmaceutical and other emerging pollutant removal. *Chemosphere* **2024**, *360*, 142312. [[CrossRef](#)]

43. Kaur, K.; Kaur, R.; Kaur, H. A systematic review of lignocellulosic biomass for remediation of environmental pollutants. *Appl. Surf. Sci. Adv.* **2024**, *19*, 100547. [[CrossRef](#)]
44. Mukherjee, A.; Borugadda, V.B.; Dynes, J.J.; Niu, C.; Dalai, A.K. Carbon dioxide capture from flue gas in biochar produced from spent coffee grounds: Effect of surface chemistry and porous structure. *J. Environ. Chem. Eng.* **2021**, *9*, 106049. [[CrossRef](#)]
45. Zhou, S.; Osman, N.B.; Li, H.; McDonald, A.G.; Mourant, D.; Li, C.-Z.; Garcia-Perez, M. Effect of sulfuric acid addition on the yield and composition of lignin derived oligomers obtained by the auger and fast pyrolysis of Douglas-fir wood. *Fuel* **2013**, *103*, 512–523. [[CrossRef](#)]
46. Hu, J.; Xiao, R.; Shen, D.; Zhang, H. Structural analysis of lignin residue from black liquor and its thermal performance in thermogravimetric-Fourier transform infrared spectroscopy. *Bioresour. Technol.* **2013**, *128*, 633–639. [[CrossRef](#)]
47. Zhou, L.; Yang, H.; Wu, H.; Wang, M.; Cheng, D. Catalytic pyrolysis of rice husk by mixing with zinc oxide: Characterization of bio-oil and its rheological behavior. *Fuel Process. Technol.* **2013**, *106*, 385–391. [[CrossRef](#)]
48. Yang, H.; Yan, R.; Chen, H.; Lee, D.H.; Zheng, C. Characteristics of hemicellulose, cellulose and lignin pyrolysis. *Fuel* **2007**, *86*, 1781–1788. [[CrossRef](#)]
49. Lou, R.; Wu, S.B. Products properties from fast pyrolysis of enzymatic/mild acidolysis lignin. *Appl. Energy* **2011**, *88*, 316–322. [[CrossRef](#)]
50. Peng, C.; Zhang, G.; Yue, J.; Xu, G. Pyrolysis of black liquor for phenols and impact of its inherent alkali. *Fuel Process. Technol.* **2014**, *127*, 149–156. [[CrossRef](#)]
51. Siipola, V.; Tamminen, T.; Källi, A.; Lahti, R.; Romar, H.; Rasa, K.; Keskinen, R.; Hyväluoma, J.; Hannula, M.; Wikberg, H. Effects of biomass type, carbonization process, and activation method on the properties of bio-based activated carbons. *Bioresources* **2018**, *13*, 5976–6002. [[CrossRef](#)]
52. Shimekit, B.; Mukhtar, H. Natural Gas Purification Technologies—Major Advances for CO<sub>2</sub> Separation and Future Directions. In *Advances in Natural Gas Technology*; Al-Megren, H.A., Ed.; INTECH: Vienna, Austria, 2012. [[CrossRef](#)]
53. Akpasi, S.O.; Isa, Y.M. Effect of operating variables on CO<sub>2</sub> adsorption capacity of activated carbon, kaolinite, and activated carbon-kaolinite composite adsorbent. *Water-Energy Nexus* **2022**, *5*, 21–28. [[CrossRef](#)]
54. Ahmad, A.; Hameed, B. Fixed-bed adsorption of reactive azo dye onto granular activated carbon prepared from waste. *J. Hazard. Mater.* **2010**, *175*, 298–303. [[CrossRef](#)] [[PubMed](#)]
55. Mochizuki, Y.; Bud, J.; Byambajav, E.; Tsubouchi, N. Pore properties and CO<sub>2</sub> adsorption performance of activated carbon prepared from various carbonaceous materials. *Carbon Resour. Convers.* **2024**, 100237. [[CrossRef](#)]

**Disclaimer/Publisher's Note:** The statements, opinions and data contained in all publications are solely those of the individual author(s) and contributor(s) and not of MDPI and/or the editor(s). MDPI and/or the editor(s) disclaim responsibility for any injury to people or property resulting from any ideas, methods, instructions or products referred to in the content.